N O T I C E

THIS DOCUMENT HAS BEEN REPRODUCED FROM
MICROFICHE. ALTHOUGH IT IS RECOGNIZED THAT
CERTAIN PORTIONS ARE ILLEGIBLE, IT IS BEING RELEASED
IN THE INTEREST OF MAKING AVAILABLE AS MUCH
INFORMATION AS POSSIBLE

NASA

Technical Memorandum 82164

Microwave Radiometric Observations Near 19.35, 92 and 183 GHz of Precipitation in Tropical Storm Cora

T. T. Wilheit, A. T. C. Chang, J. L. King, E. B. Rodgers, R. A. Nieman, B. M. Krupp, A. S. Milman, J. S. Stratigos and H. Siddalingaiah

MICROWAVE RADIOMETRIC OBSERVATIONS NEAR 19.35, 92 and 183 GHz OF PRECIPITATION IN TROPICAL STORM CORA

T. T. Wilheit, A. T. C. Chang, J. L. King and E. B. Rodgers
NASA/Goddard Space Flight Center
Greenbelt, Maryland

R.A. Nieman
Computer Sciences Corporation
Silver Spring, Maryland

B.M. Krupp and A.S. Milman
Systems and Applied Sciences Corporation
Riverdale, Maryland

J.S. Stratigos
Georgia Institute of Technology
Atlanta, Georgia

H. Siddalingaiah
OAO Corporation
Beltsville, Maryland

ABSTRACT

Observations of rain cells in the remains of a decaying tropical storm were made by Airborne Microwave Radiometers at 19.35, 92 and three frequencies near 183 GHz. Extremely low brightness temperatures, as low as 140°K were noted in the 92 and 183 GHz observations. These can be accounted for by the ice often associated with raindrop formation. Further, the 183 GHz observations can be interpreted in terms of the height of the ice. The brightness temperatures observed suggest the presence of precipitation sized ice as high as 9 km or more.

MICROWAVE RATIOMETRIC OBSERVATIONS NEAR 19.35, 92 AND 183 GHz OF PRECIPITATION IN TROPICAL STORM CORA

INTRODUCTION

Precipitation, particularly rain, is probably the most fundamental meteorological parameter. It is a primary determinant of the quality of human life via an entire spectrum of issues ranging from crop yields to the planning of picnics. Further, the latent heat release associated with rain is a significant term in the energy budget of the atmosphere and thus exerts an important influence on day-to-day weather. The understanding and prediction of weather and climate require good precipitation data. Throughout much of the world's land area there are direct measurements of rain, but these measurements are unevenly distributed and because of the highly variable character of rain, sampling problems are endemic. Over the oceans, direct rain measurements are almost non-existent. In order to arrive at global precipitation data with adequate sampling, spaceborne remote sensing techniques are required.

A host of visible and infrared techniques (Barrett, 1970, 1973; Martin and Scherer, 1973; Martin et al., 1975; Follansbee and Oliver, 1975; Scofield and Oliver, 1977; Griffith et al., 1978) have been developed based on empirical relationships between cold and/or bright clouds and rainfall. Many of these techniques show promise but all have their limitations as well. Wilheit et al. (1977) have developed a passive microwave technique, for measuring rainfall using wavelengths of the order of 1 to 2 cm, which is based on a causal model. Many aspects of this technique need refinement but its most serious limitation is that it only works over water surfaces. Although rain over water is important, clearly, rain over land is of more general interest. A passive microwave technique using measurements at 37 GHz (0.8 cm) for measurement of rain over land was developed by Savage and Weinman (1975) and was tested by Rodgers et al. (1979). This technique is based on the scattering of microwave by the hydrometeors near the top of the rain column, but it proved to be marginal for mapping rain and demonstrated no capability for measuring rainfall intensity. Nevertheless, the tests

indicated that the basic physical reasoning was sound. The investigation reported here is based on an attempt to enhance the scattering mechanism used by Savage and Weinman by going to higher frequencies (shorter wavelengths). 92 GHz (0.33 cm) and 183 GHz (0.16 cm). The scattering is substantially independent of polarization, whereas variations in surface properties are reflected much more strongly in horizontal polarization brightness temperatures than in vertical. Thus vertical polarization (at a 45° view angle) was chosen to enhance scattering vis-a-vis surface effects in the observed brightness temperature. Although a technique for measuring rain over land was sought, the experiment was directed to rain over ocean so that measurements at 19.35 GHz could serve as rain truth (a la Wilheit et al. 1977) and to reduce the aircraft altitude requirements to be consistent with an airplane which could carry the crew needed to operate a very experimental collection of instruments. At rain rates greater than a few mm/hr the atmosphere is substantially opaque at 92 and 183 GHz so the ocean background does not affect the observed radiances.

On the basis of these same expectations (Burke et al., 1981), a new sensor, a microwave imager (SS/MI) has been developed for the Defense Meteorological Satellite Program (DMSP). This new sensor, which is currently planned for a 1984 launch, has an 85 GHz vertically polarized channel. This should respond essentially like the 92 GHz radiometer reported here.

Table 1
Microwave Radiometers

Frequency (GHz)	View/Angle	Polarization	Beamwidth	Comments
19.35	−50 to +50	H	2.8°	A/C ESMR
94	45	V	6°	
183.1 ± 1.2	45	V	6°	
183.1 ± 5.0	45	V	6°	Single Instrument
183.1 ± 9.0	45	V	6°	

Microwave Radiometers

This paper deals with the measurements from 5 microwave radiometers aboard the CV-990 aircraft; their important parameters are given in table I. Note that all are fixed beam viewing 45° to the right side of the aircraft except for the 19.35 GHz Electrically Scanned Microwave Radiometer (Aircraft Model), A/C ESMR, which scans from 50° to the left, through nadir to 50° to the right in 39 steps every 2 seconds. The polarization vector of the A/C ESMR is parallel to the aircraft velocity vector so that the polarization is horizontal except at nadir where the definitions of the two polarizations break down. The 92 GHz channel observes vertically polarized radiation making scattering more easily detectable by reducing brightness temperature changes due to changes of surface composition. The polarization of the 183 GHz channels is irrelevant because the atmosphere is unpolarized and essentially opaque near the very strong water vapor line at 183.1 GHz.

All these radiometers here employ superhetrodyne receivers with no image rejection so they detect radiation over two bands separated by distances above and below the listed center frequency. For the three channels centered near the 183 GHz water vapor line, the radiometer center frequency is chosen to coincide with the water vapor line frequency to take advantage of the near symmetry of molecular resonance lines. Thus the channel listed as 183.1 ± 1.2 GHz receives energy in two bands centered at 181.9 and 184.3 GHz and similarly for the other two 183 GHz channels. The width of each of these bands is about 20% of its separation from the line center.

The 19.35 GHz radiometer is calibrated by electrically switching to waveguide terminations at widely spaced, known temperatures (ambient and liquid nitrogen). The high frequency (92 to 183 GHz) radiometers are constructed in a single unit which includes a reflector which can be moved to enable the instrument to view the atmosphere, or either of two calibration targets (heated to +70°C or cooled to -30°C). The calibration accuracy of all the fixed beam radiometers is thought to be within 5° and the A/C EMSR to be 10° at nadir.

Flight Lines

The best opportunity for observing rain with this system came on August 11, 1978 during Tropical Storm Cora. Cora had developed from a disturbance off the African coast on August 4,

3

intensified to hurricane status (maximum winds were estimated a 40 m/s) on August 9 and quickly dissipated west of the Antilles (Lawrence, 1979). At the time of the flight the center was located near 12°N 66°W (off the coast of Venezuela). The NASA CV-990 took off from San Juan at 1609Z and flew directly to the storm and began the pattern indicated in figure 1 at 1650Z at an altitude of 11 km. The flight continued from there straight south across the nominal center of the storm and then counter-clockwise one and a quarter times in an octagonal pattern centered on the storm. The flight path then became somewhat chaotic as the pilot executed repeated passes near several rain cells and climbed to an altitude of 12 km. This segment is shown in more detail in figure 2. The wind arrows, placed at 2-minute intervals along the track in Figure 1, indicate the decadent character of the storm as there is no longer any closed circulation, only a weak wave in the easterly wind pattern. Rain was only noted near the northern vertex of the octagon pattern. The aircraft completed the pattern indicated at 1855Z and returned to San Juan landing at approximately 1930Z.

Rawinsonde observations were taken at Curacao Island located at approximately 12.4°N 69.0°W and just southwest of Cora at 1200 GMT on August 11 and 0000 GMT on August 12. Because of the location of the sounding with respect to Cora's position, the sounding is somewhat representative of Cora's environment. The rawinsonde observations revealed a slightly warmer tropospheric layer than that of the average tropical troposphere, a troposphere whose lapse rate was conditionally unstable, became more moist, particularly at 700 mb and above 500 mb during the day as Cora moved westward. The soundings also revealed a convective cloud level (CCL) of approximately 940 mb (1.4 km), a tropopause height of 130 mb (15.4 km), and a freezing level at 560 mb (4.9 km). Assuming thermodynamic equilibrium at the cloud tops for clouds whose emissivity were equal to one, the maximum cloud heights estimated from the GOES-East infrared images and Curacao Island rawinsonde data were estimated to be near the tropopause (15 km) over much of the area in which the CV-990 flew. Wind speed and directions at the upper tropospheric level were generally easterly at less than 10 kts at Curacao Island and easterly at 30 kts over Cora as measured by CV-990.

Observations

Figures 3-6 present the observations of the various microwave radiometers near the northern vertex of the octagon pattern. The data from the first two passes through the area are shown in Figures 3 and 4 while Figures 5 and 6 display the data from the period when the aircraft flew over individual cells. The data shown are restricted to periods where the aircraft roll angle was less than 5° for more than half a minute. Additional gaps are introduced into the 92, 183 GHz data at approximately 3-minute intervals by the calibration cycle and at random intervals by instrument malfunctions.

The 19.35 GHz data are displayed both as an image and as a line trace of the 45°R beam position. Brightness temperatures greater than 210°K represent rain of approximately 2 mm/hr or more. Lighter rain or heavy clouds would fall roughly in the 170 to 200°K range with light clouds and clear skies below 170°K. The calibration of the images is such that the medium and very dark tones represent rain. The area viewed by the 92 and 183 GHz radiometers is along the bottom edge of the image. The feature at 1820Z is typical of the observations. Here we see 9? GHz brightness temperatures as low as 150°K in the neighborhood of a rain cell as indicated on both the 19.35 GHz image and trace. Similar, but not identical, features are seen on the three 183 GHz channels. The principal purpose of the theory section will be to explain the existence of such features. It is then less of a problem to explain situations like 1828Z where the cold features at 92 and 183 GHz do not correspond to rain in the 1935 GHz trace or vice-versa (1852Z). This will be left to the discussion section. For the remainder of the flight, which is not shown here, there was neither any indication of rain on the 19.35 GHz radiometer nor brightness temperature below 240°K observed by any of the 92 and 183 GHz radiometer channels.

Theory

The basic model used for calculating microwave brightness temperatures in raining situations is illustrated in Figure 7. In this model, a Marshal-Palmer (1948) distribution of liquid water droplets is assumed from the 0°C isotherm (freezing level) to the surface. The assumed relative humidity

increases linearly with height from 80% at the surface to 100% at the freezing level and above. For a variable thickness above the freezing level, an ice layer is assumed with the same partic. size distribution as the liquid droplets below the freezing level. The shape of the temperature profile is assumed to be U.S. Standard (AFCRL 1965) with a constant temperature addition to adjust the freezing level. The lapse rate is thus $-6.5°C/km$ up to 11 km: nothing above that altitude is important for the frequencies considered here. The adjustable parameters of the model are freezing level (set at 5 km for the present paper), rain rate (through the M-P distribution) and thickness of the ice layer. This model differs from that used by Wilheit *et al.* (1977) for the interpretation of 19.35 and 37 GHz measurements in two respects. First, in saturating the atmosphere with water vapor above the freezing level and second, in adding the variable thickness ice layer. Both of these details were irrelevant to the Wilheit *et al.* (1977) purposes but, as will be seen, are critical to interpreting the observations of the previous section. The ice layer is physically required because the ice phase is usually required for rain drop formation. The ice free case must also be retained because in tropical conditions precipitation sometimes forms without an ice phase (Pruppacher and Klett, 1978). The equation of radiative transfer is solved in the same manner as described by Wilheit *et al.* (1977), but with programming changes to assure timely convergence of the iterations.

A word of caution is necessary at this point. The ice-free model worked well as a quantitative measure of rain rate and should also work for any other situation where the ice is unimportant. However, it cannot be asserted that the ice as described here is related in any clear way to the rain intensity. The coupling between the rain rate and the ice distribution is merely a convenient way to exercise the ice particle size and density through physically reasonable ranges. It is for this reason that the abscissae of all appropriate figures are labeled in mean radius and particle density in addition to rain rate.

In Figure 8, the brightness temperatures resulting from this model at 19.35 GHz are presented. Note that at this frequency there is virtually no sensitivity to the ice layer thickness at low to medium rain rates thus supporting the assumptions of Wilheit *et al.* (1977).

Figures 10-13 give the results from the same model for 92 GHz, 183 ± 1.2, 183 ± 5 and 183 ± 9 GHz respectively. Consider, for the moment, only the zero ice thickness cases. These represent

substantially the Wilheit *et al.* (1977) model which was reasonably successful in accounting for the observations at 19.35 and 37 GHz; clearly these results are not even in qualitative agreement with the observations of the previous section. With so profound a discrepancy, varying the parameters of the ice-free model would not be a fruitful exercise; a basic qualitative difference is required. The brightness temperatures observed, being substantially below the thermometric temperature of any part of the atmosphere, require an emissivity much less than unity. Because of the opacity of the liquid rain layer, the reflectivity of the surface cannot contribute to this low emissivity. However, scattering from hydrometeors can also reduce the emissivity. This can be seen even in the 19.35 GHz calculations; for high rain rates, the brightness temperature is somewhat less than 273°K (0°C) but all constituents having a significant role in the radiative transfer process have thermometric temperatures greater than this. The scattering by liquid hydrometeors however is far too weak *vis-a-vis* absorption and reradiation to account for the dramatic emissivity decrease observed. To account for the observed low emissivity, the balance between the scattering and absorption must be drastically shifted in favor of scattering. In terms of physical optics, this means that the ratio of the real to the imaginary part of the index of refraction of the hydrometeors must become much larger. Using the dielectric measurements of Lane and Saxton (1952) as summarized by Chang and Wilheit (1979) the index of refraction of liquid water at 92 GHz and −10°C is 2.7 + 1.1 i whereas that for ice is $1.8 + 5 \times 10^{-4}$ i.

In Figure 9, it can be seen that an assumed ice layer thickness of about 1 km or greater explains the low observed brightness temperatures at 92 GHz. Similarly, Figures 11 to 13 show the effect of ice at the three frequencies near 183 GHz. Note that the response at 183 ± 9 GHz and 183 ± 5 GHz is similar to the 92 GHz response in that they show a continually decreasing brightness temperature up to a thickness of 5 km but the 183 ± 1.2 GHz shows no consequential decrease until the thickness exceeds 4 km. This effect, caused by the opacity due to the atmospheric water vapor, provides approximate information as to the height to which precipitation sized ice is being lifted in the convective cells.

Discussion

The 19.35 GHz and 92 GHz data between1728Z and 1734Z(Figure 5) provide a straightforward example in support of the theory developed in the previous section. The rain rate increases and decreases indicated by the 19.35 GHz data are matched almost one-for-one by decreases and increases in the brightness temperatures at 92 GHz. Unfortunately the 183 GHz data are missing due to an instrument malfunction here. The feature at1652Z(Figure 4) provides another example. Here all radiometer channels are working. The fact that the features shows even at 183 ± 1.2 GHz suggests that ice is being lifted to more than 9 km (5 km freezing level plus 4 km ice layer thickness). The features of 92 and 183 GHz are not quite coincident with the rain area indicated in the 19.35 GHz data. Such displacements occur throughout the data and may be accounted for with proper allowance for the viewing geometry, the storm geometry with winds of the same order of magnitude as the maximum fall speeds (ca. 10 m/s); and the fact that the 19.35 GHz is responding to the liquid hydrometeors and the 92 and 183 GHz channels are responding to the frozen hydrometeors.

The feature at 1842Z (Figure 6) is especially interesting. The aircraft approached the cell from the southeast flying almost parallel to the wind. The 19.35 GHz showed the first indication of rain followed almost immediately by a sharp decrease in the 92-183 GHz brightness temperature indicating ice. As the flight line continued past the rain maximum, the 92 GHz brightness continued to drop indicating an increasing amount of scattering from the ice which could be caused by either an increase in the size or number of ice particles. The various 183 GHz channels then began to show less scattering by the ice suggesting that the ice was falling back down from the approximately 10 km or higher altitude it had reached. Thus the 183 GHz channels provide a vertical view of the frozen hydrometeors.

Features such as those between 1845Z and 1855Z (Figure 6) provide a counter-example to a glib over interpretation of these data. There are several indications of rain in the 19.35 GHz data but little indication of ice in the 92 and 183 GHz data. The extent and shapes of these rain features make geometric explanations of the lack of ice unsatisfying; these are probably examples of rain drop formation with little or no ice phase.

8

Data have been presented which showed that at 92 and 183 GHz extremely low (as low as 140°K) brightness temperatures are observed in association with rain. It has been shown through radiative transfer modelling that these low brightness temperatures can be accounted for by the ice phase commonly associated with the rain drop formation process and that the 183 GHz channels used here can be used to infer the maximum height of these frozen hydrometeors. A scanning version of this instrument has been built for use on high altitude (20 km) aircraft. This should provide insight into the physics of convective rainfall. In combination with a radiometer at 19.35 GHz it also is able to distinguish ice phase from non-ice phase (warm) precipitation over tropical oceans. Similarly, the 85 GHz channel of the SSMI on DMSP which will be launched in 1984 can be used to detect ice phase precipitation.

REFERENCES

1. Air Force Cambridge Research Laboratory (AFCRL) (1965), Handbook of Geophysics and and Space Environments, McGraw-Hill, New York.

2. Barrett, E. C., 1970, "The estimation of monthly rainfall from satellite data," Mon. Wea. Rev., 98, 322-327.

3. Barrett, E. C., 1973, "Forecasting daily rainfall from satellite data," Mon. Wea. Rev., 101, 215-222.

4. Burke, H. K., K. R. Hardy, N. K. Tripp (1981), "Detection of Rainfall Rates Utilizing Space-borne Microwave Radiometers," presented at Workshop on the Measurement of Precipitation from Space held at Goddard Space Flight center, April 1981.

5. Chang, A. T. C., and T. Wilheit (1979), "Remote sensing of atmospheric water vapor, liquid water, and wind speed at the ocean surface by passive microwave techniques from the Nimbus 5 satellite, Radio. Sci., 14(5), 793-802.

6. Follansbee, W. A., and V. J. Oliver, 1975: "A comparison of infrared imagery and video pictures in the estimation of daily rainfall from satellite data," NOAA Tech. Memo, NESS 62, 14 pp.

7. Griffith, G. C., W. L. Woodley, S. Browner, J. Tiejeiro, M. Maier, D. W. Martin and D. N. Sikdar, 1978: "Rain estimation from geosynchronous satellite imagery — visible and infrared studies," Mon. Wea. Rev., 106, 1153-1171.

8. Lane, J. A., and J. A. Saxton (1952), "Dielectric dispersion in pure polar liquids at very high radio frequencies," Proc. Roy. Soc. London. Ser. A, 214, 531-545.

9. Lawrence, M. B., 1979; "Atlantic Hurricane Season of 1978," Mon. Wea. Rev., 107, 477-491.

10. Marshall, T. S., and W. M. Palmer (1948), "The distribution of raindrops with size," J. Meteorol., 5, 165-166.

11. Martin, D. W., and W. D. Scherer, 1973: "Review of satellite rainfall estimation methods," Bull. Amer. Meteor. Soc., 54, 661-674.

12. Martin, D. W., J. Stout and D. N. Sikdar, 1975: GATE area rainfall estimation from satellite images,": Report NOAA Grant 04-5-158-47, University of Wisconsin, 28 pp.

13. Pruppacher, H. R., and J. D. Klett (1978): "Microphysics of clouds and precipitation," D. Reidel Publishing Co., Boston, pp. 5-7.

14. Rodgers, E. B., H. Siddalingaiah, A. T. C. Chang, T. T. Wilheit (1979), "A Statistical Technique for Determining Rainfall over Land Employing Nimbus-6 ESMR Measurements," J. App. Met, 18, 987-991.

15. Savage, R. C., and J. A. Weinman, 1975: "Preliminary calculations of the upwelling radiance from rain clouds at 37.0 and 19.35 GHz," Bull. Amer. Meteor. Soc., 56, 1272-1274.

16. Scofield, R. A., and V. J. Oliver, 1977: "A scheme for estimating convective rainfall from satellite imagery," NOAA Tech. Memo., NESS 86, 47 pp.

17. Wilheit, T. T., A. T. C. Chang, M. V. Rao, E. B. Rodgers and J. S. Theon, 1977: "A satellite technique for quantitatively mapping rainfall rate over the oceans," J. Appl. Meteor., 16, 551-560.

ACKNOWLEDGMENTS

Table II
Offsets and Frequencies used in Figures 3-6

| Symbol	Frequency	Offset
A	92 GHz	0°K
B	183.3 ± 1.2 GHz	100°K
C	183.3 ± 5.0 GHz	200°K
D	183.3 ± 9.0 GHz	300°K
E	19.35 GHz	600°K

Figure Captions

1. Flight path of NASA CV-990 through tropical storm Cora. Wind barbs are in knots.

2. Expanded view of a portion of the flight path of the NASA CV-990.

3. Brightness temperatures observed by various radiometers aboard NASA CV-990 with offsets to improve readability (See Table II). 1648Z to 1710Z

4. Brightness temperatures observed by various radiometers aboard NASA CV-990 with offsets to improve readability (See Table II). 1724Z to 1741Z

5. Brightness temperatures observed by various radiometers aboard NASA CV-990 with offsets to improve readability (See Table II). 1813Z to 1830Z

6. Brightness temperatures observed by various radiometers aboard NASA CV-990 with offsets to improve readability (See Table II). 1833Z to 1853Z

7. Model used for radiative transfer calculations.

8. Brightness temperature calculations for 19.35 GHz. Numbers adjacent to curves indicate thickness of ice layer. The assumed freezing level is 5 km.

9. Brightness temperature calculations for 92 GHz. Numbers adjacent to curves indicate thickness of ice layer. The assumed freezing level is 5 km.

10. Brightness temperature calculations for 183 ± 1.2 GHz. Numbers adjacent to curves indicate thickness of ice layer. The assumed freezing level is 5 km.

11. Brightness temperature calculations for 183 ± 5.0 GHz. Numbers adjacent to curves indicate thickness of ice layer. The assumed freezing level is 5 km.

12. Brightness temperature calculations for 183 ± 9.0 GHz. Numbers adjacent to curves indicate thickness of ice layer. The assumed freezing level is 5 km.
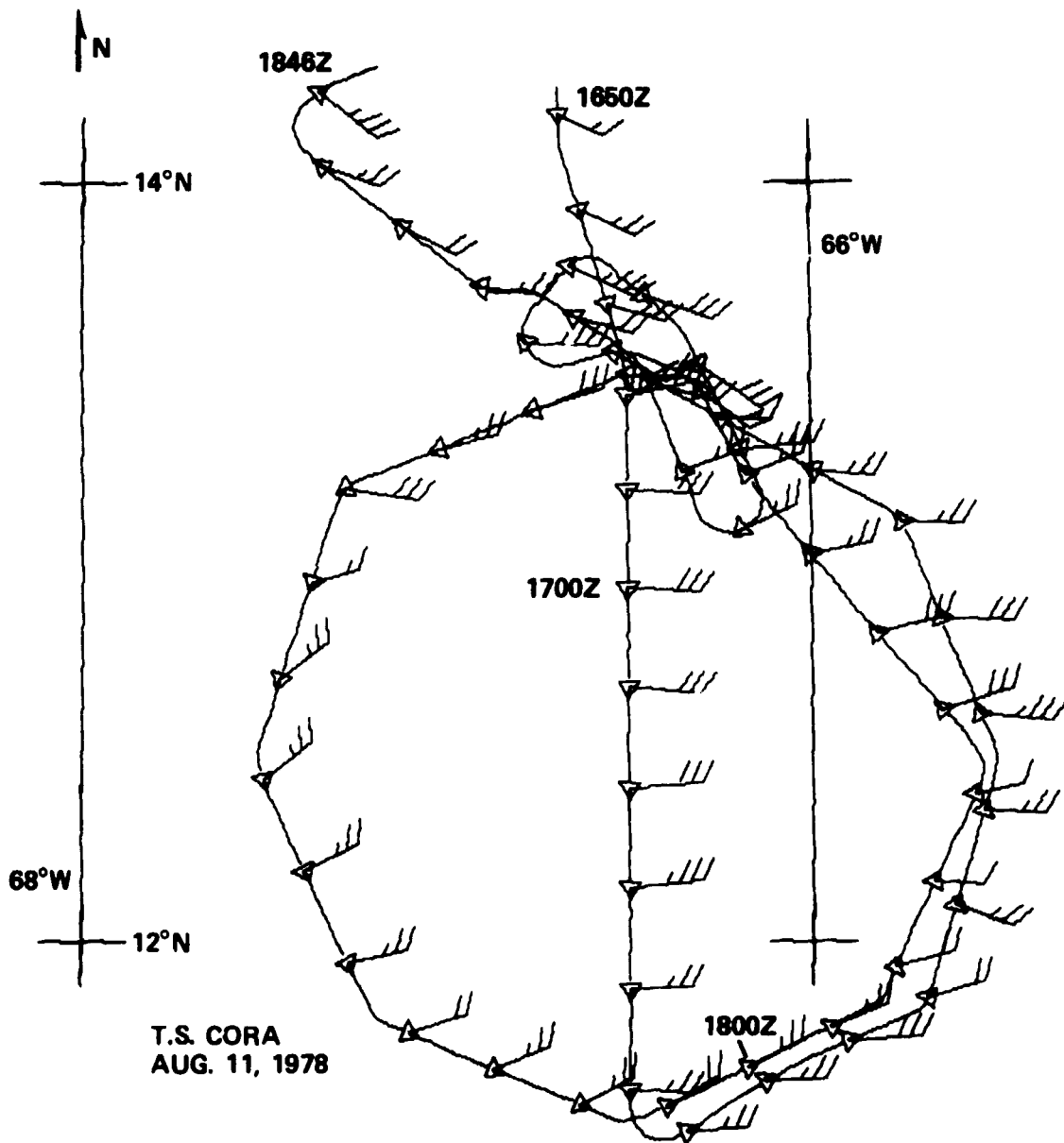
Figure 1. Flight path of NASA CV-990 through tropical storm Cora. Wind barbs are in knots.
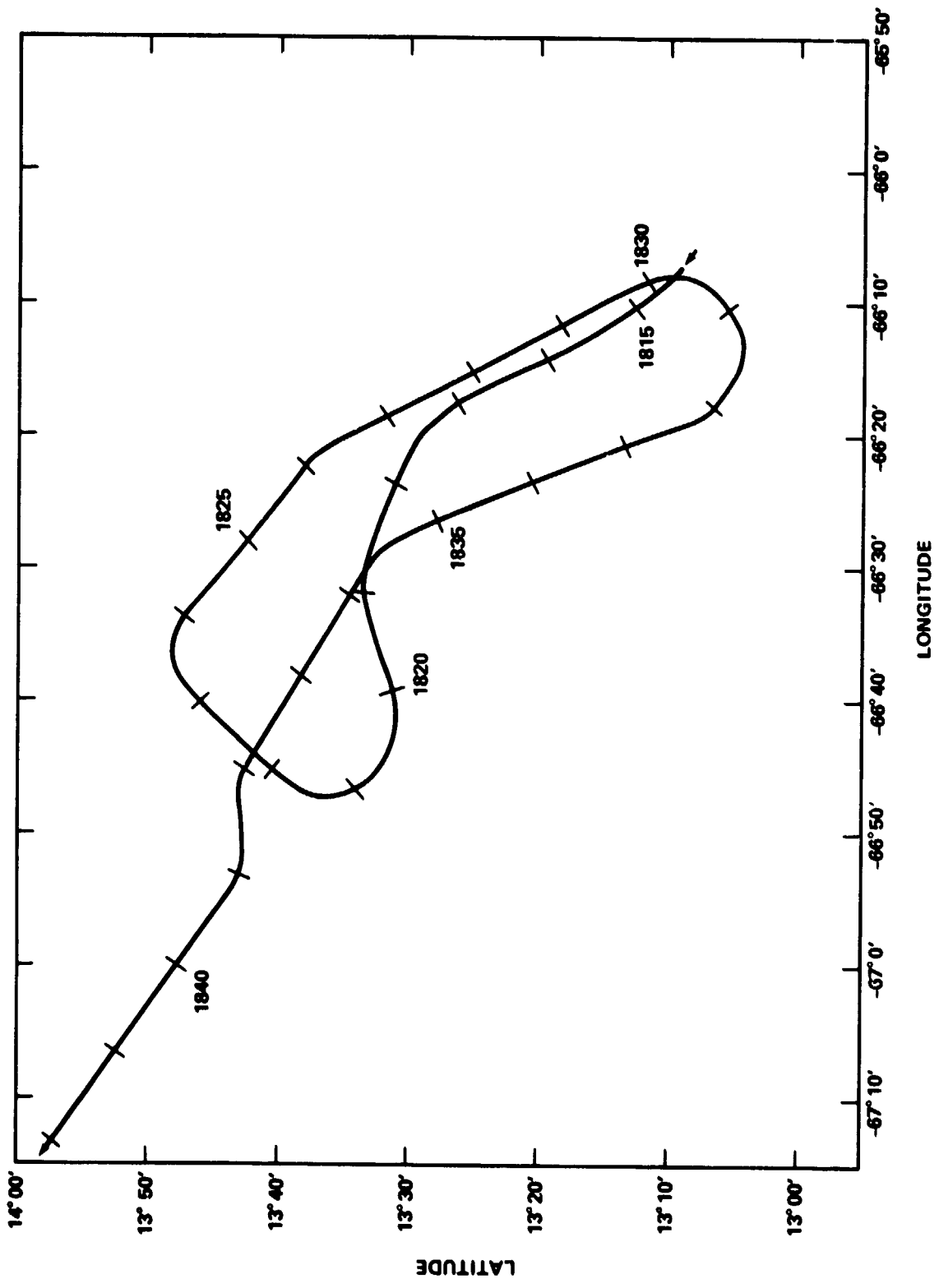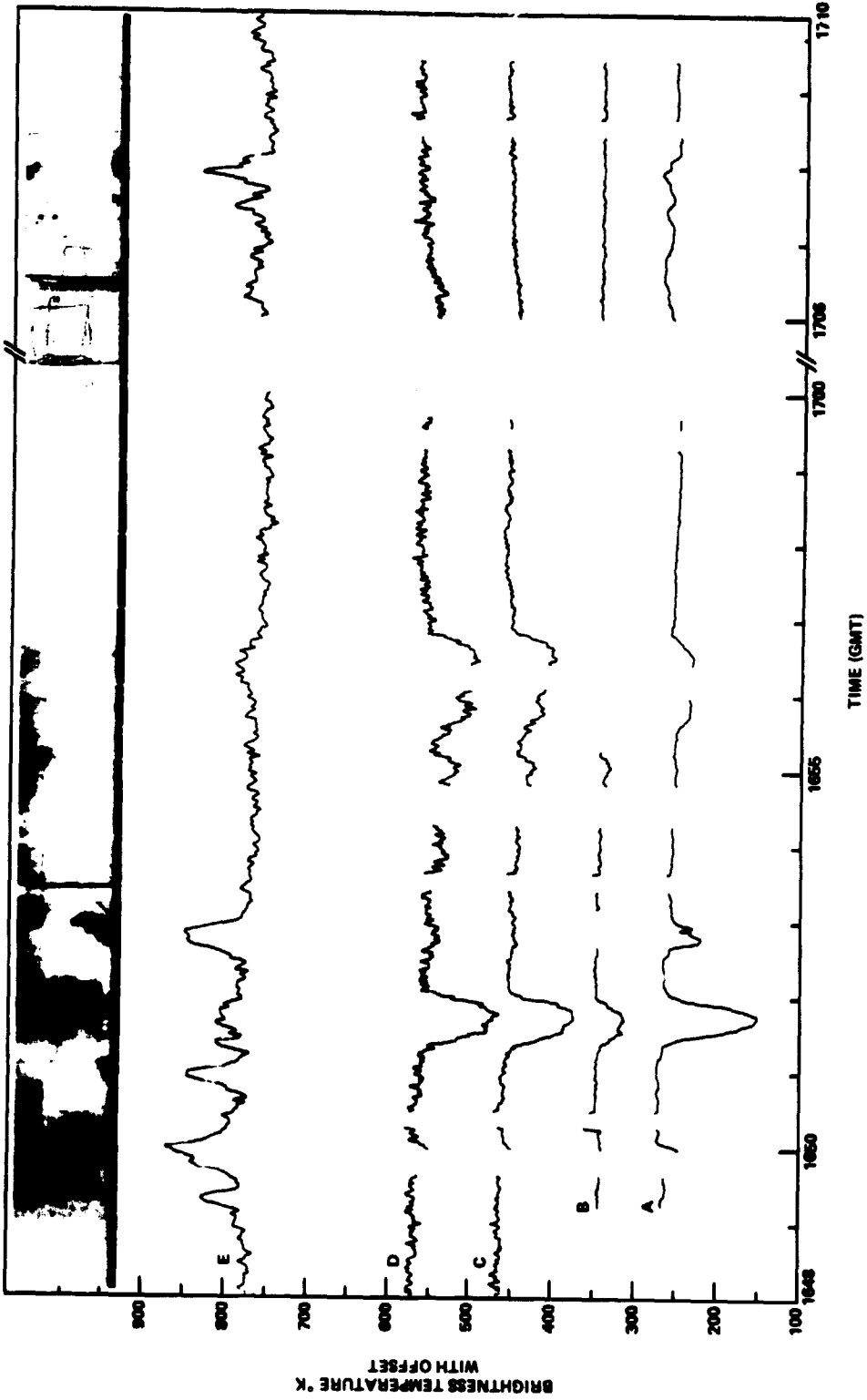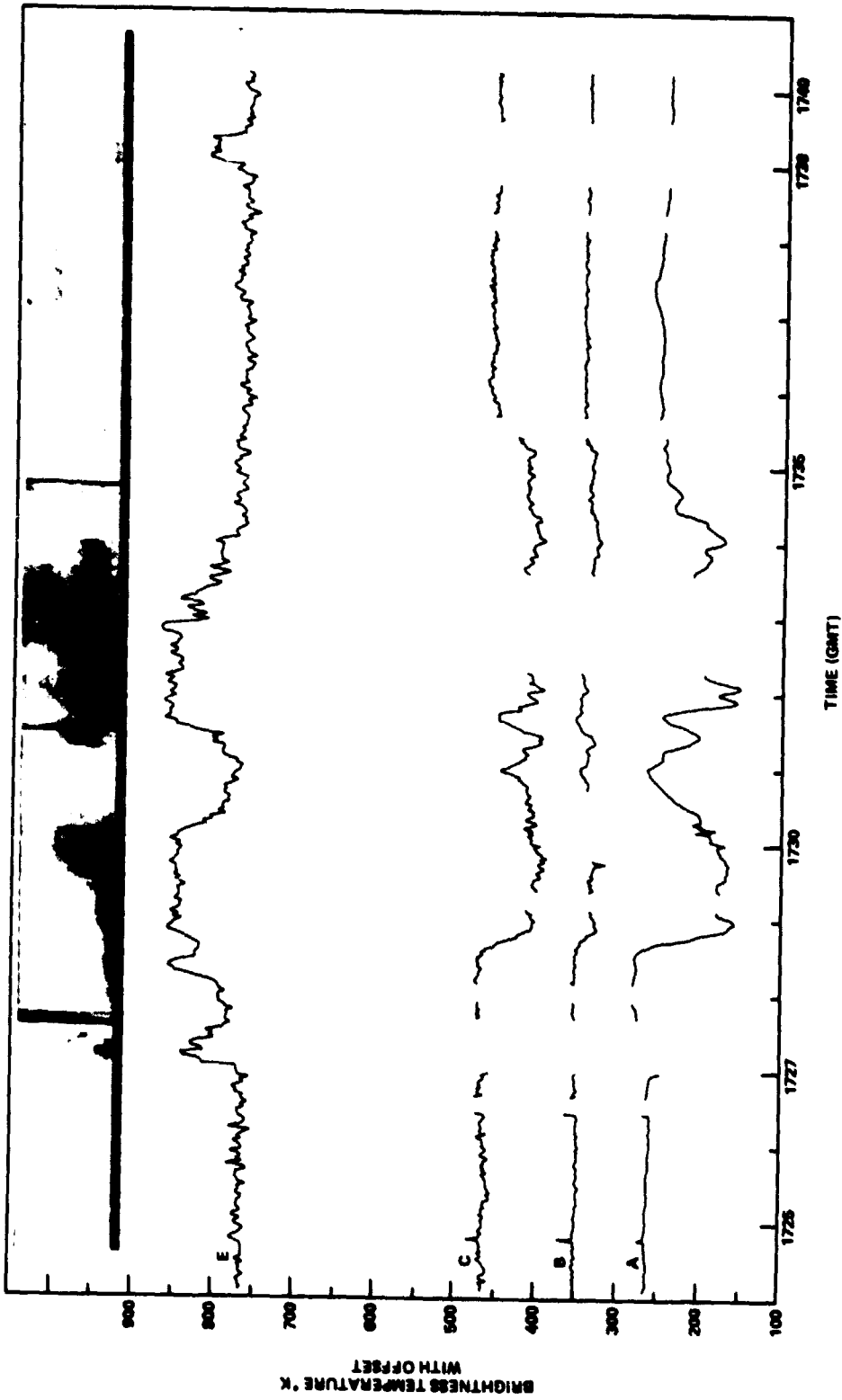
Figure 2. Expanded view of a portion of the flight path of the NASA CV-990.

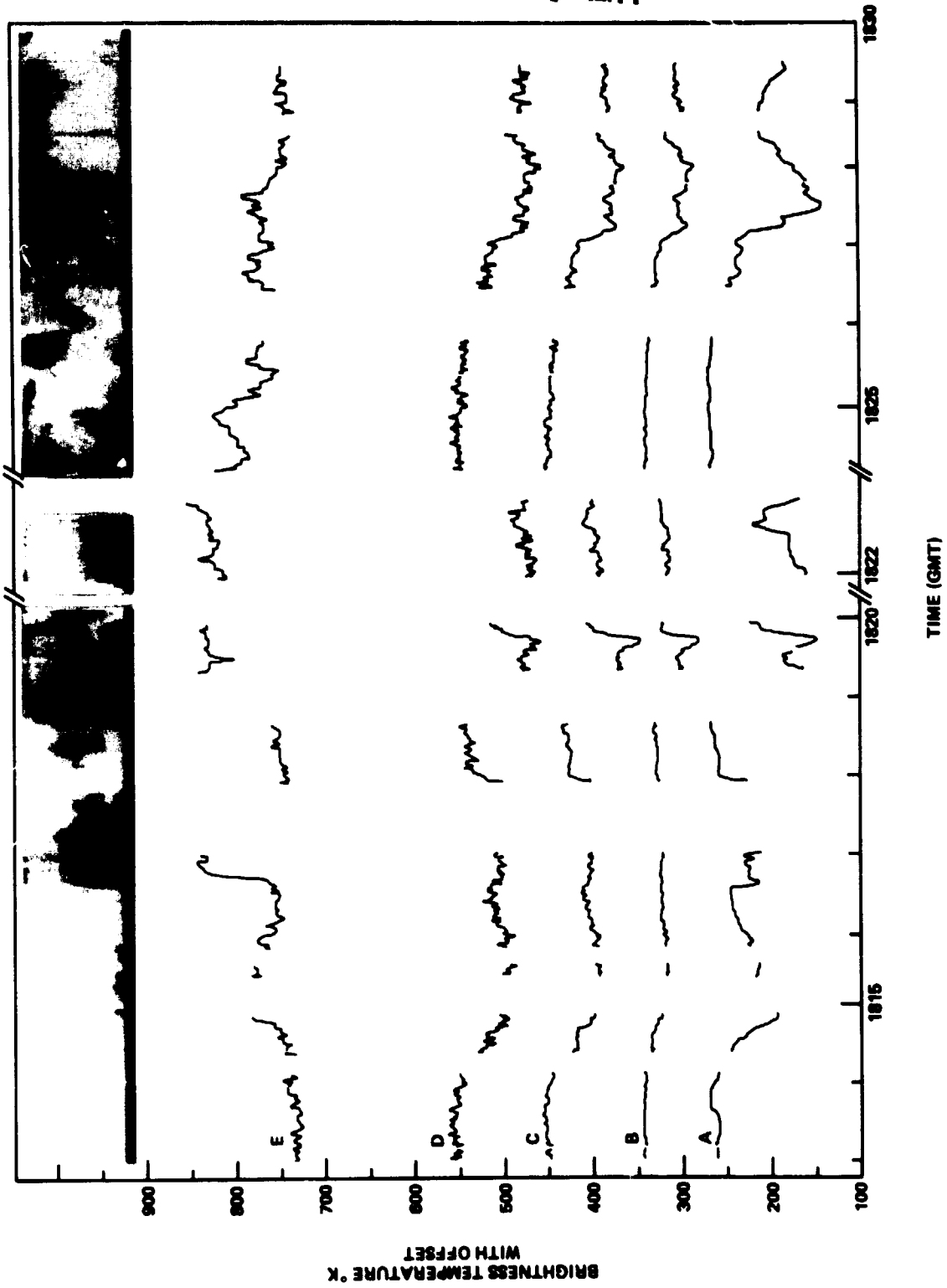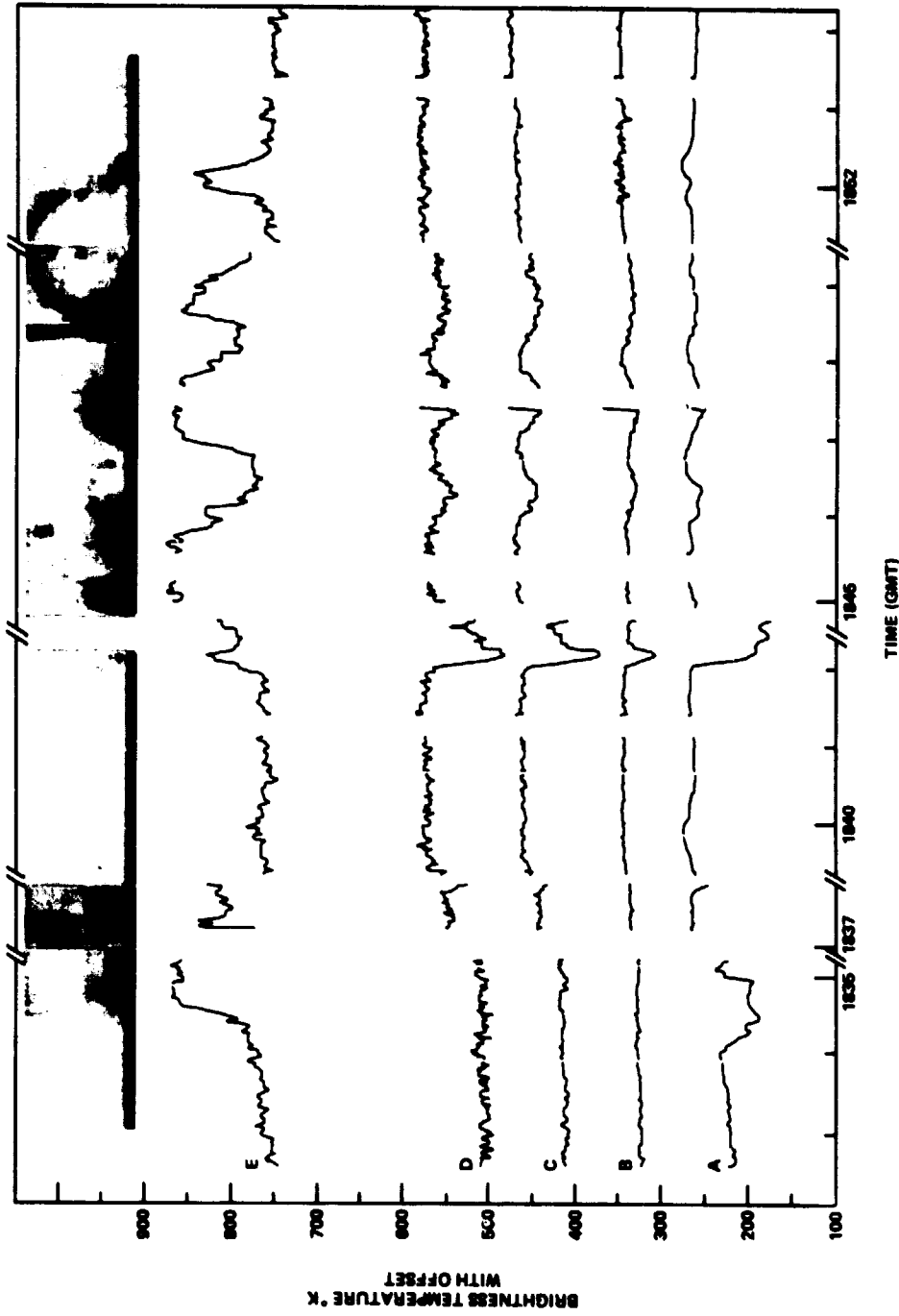Figure 3. Brightness temperatures observed by various radiometers aboard NASA CV-990 with offsets to improve readability (See Table II). 1648Z to 1710Z
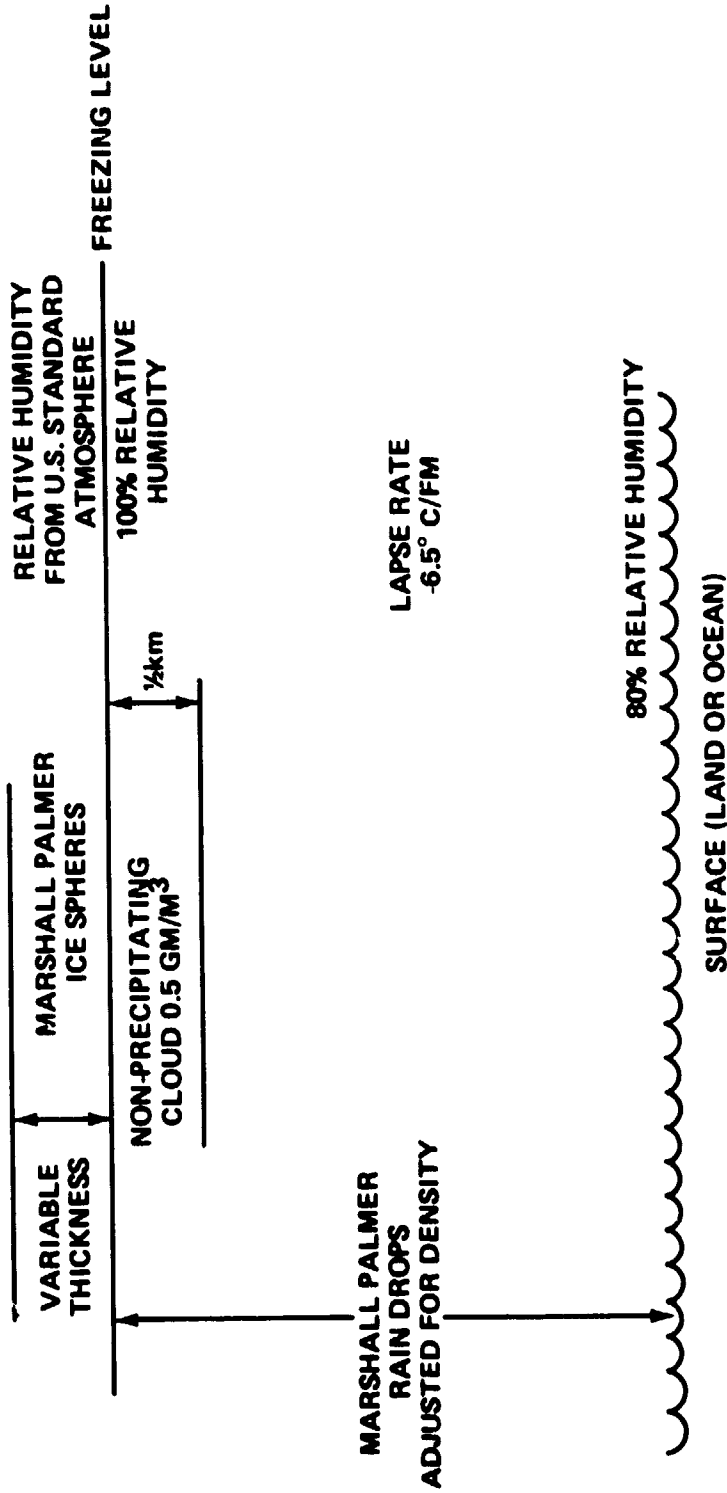
Figure 4. Brightness temperatures observed by various radiometers aboard NASA CV-990 with offsets to improve readability (See Table II). 1724Z to 1741Z

Figure 5. Brightness temperatures observed by various radiometers aboard NASA CV-990 with offsets to improve readability (See Table II). 1813Z to 1830Z

Figure 6. Brightness temperatures observed by various radiometers aboard NASA CV-990 with offsets to improve readability (See Table II). 1833Z to 1853Z

VARIABLE
THICKNESS

MARSHALL PALMER
ICE SPHERES

RELATIVE HUMIDITY
FROM U.S. STANDARD
ATMOSPHERE

FREEZING LEVEL

NON-PRECIPITATING
CLOUD 0.5 GM/M^3

¼km

100% RELATIVE
HUMIDITY

LAPSE RATE
-6.5° C/FM

MARSHALL PALMER
RAIN DROPS
ADJUSTED FOR DENSITY

80% RELATIVE HUMIDITY

SURFACE (LAND OR OCEAN)

Figure 7. Model used for radiative transfer calculations.
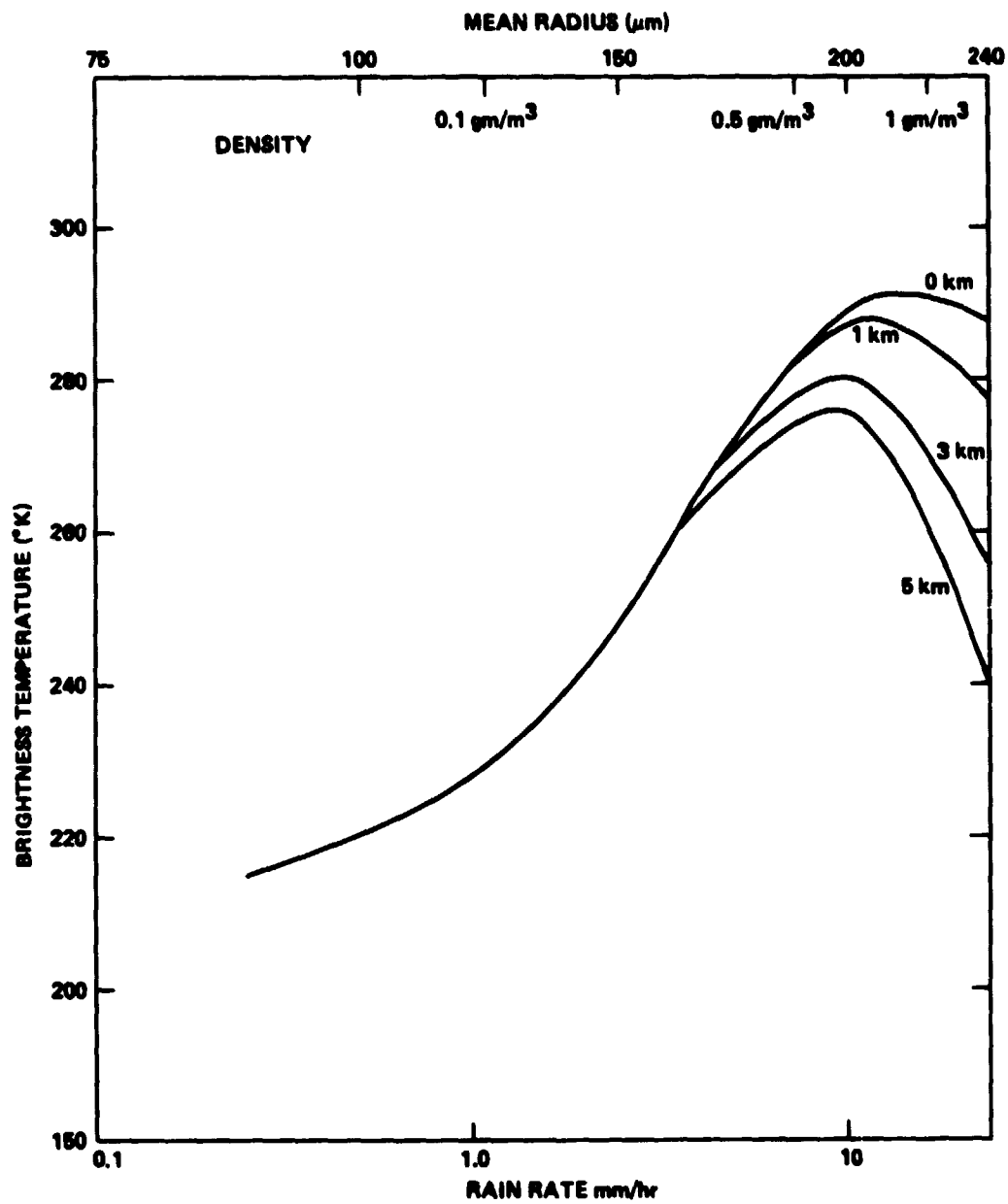
Figure 8. Brightness temperature calculations for 19.35 GHz. Numbers adjacent to curves indicate thickness of ice layer. The assumed freezing level is 5 km.
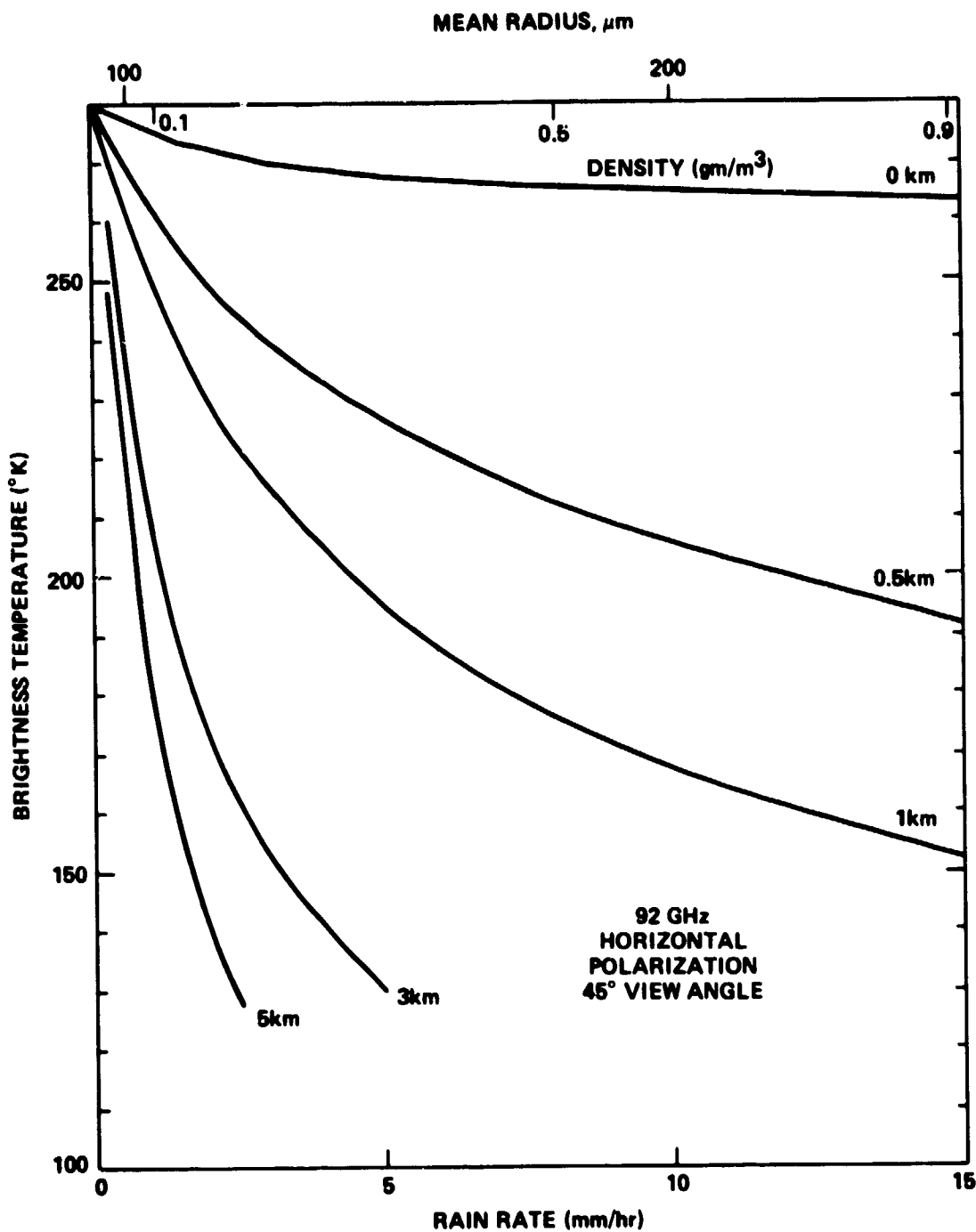
Figure 9. Brightness temperature calculations for 19.35 GHz. Numbers adjacent to curves indicate thickness of ice layer. The assumed freezing level is 5 km.
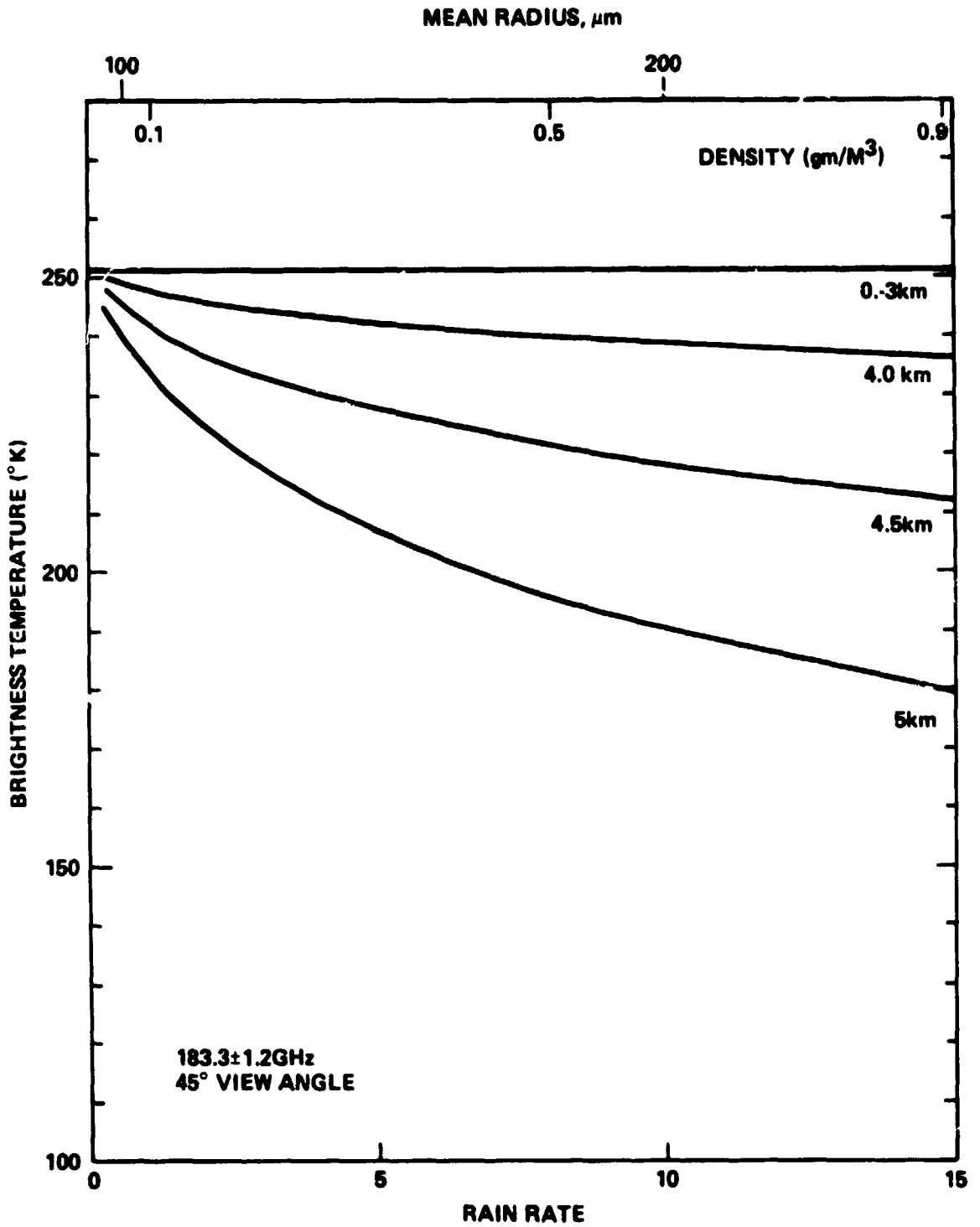
Figure 10. Brightness temperature calculations for 183 ± 1.2 GHz. Numbers adjacent to curves indicate thickness of ice layer. The assumed freezing level is 5 km.
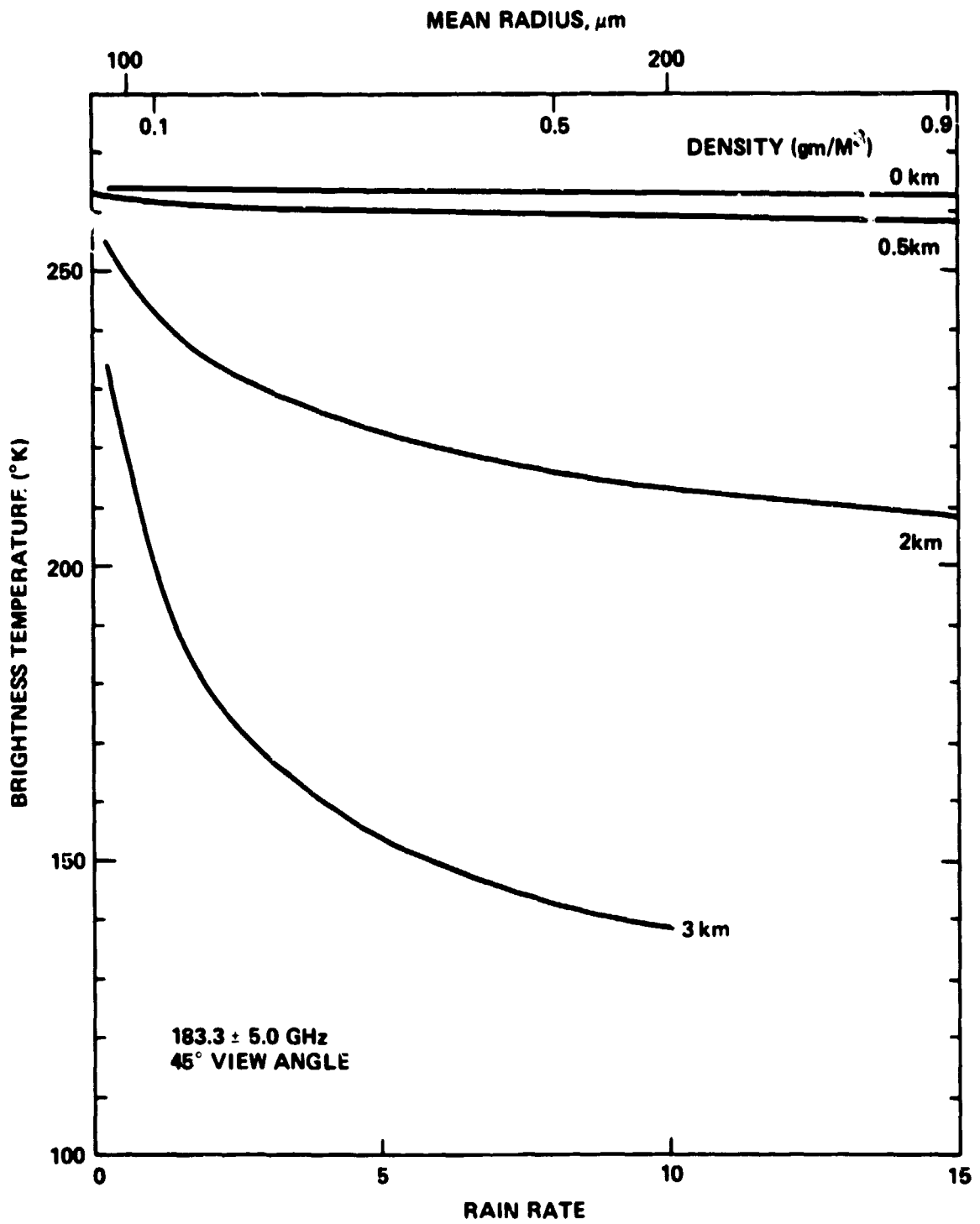
Figure 11. Brightness temperature calculations for 183 ± 5.0 GHz. Numbers adjacent to curves indicate thickness of ice layer. The assumed freezing level is 5 km.
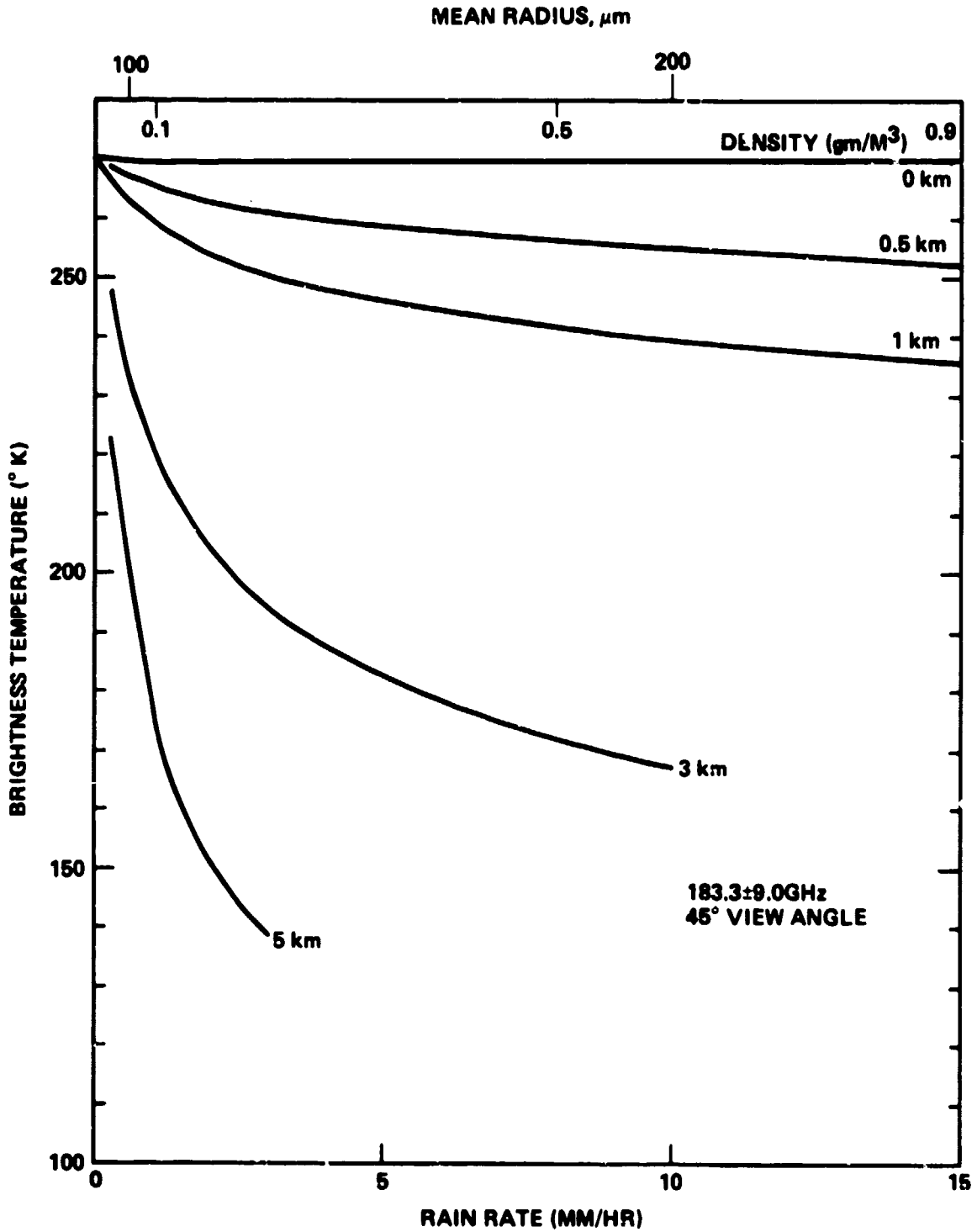
Figure 12. Brightness temperature calculations for 183 ± 9.0 GHz. Numbers adjacent to curves indicate thickness of ice layer. The assumed freezing level is 5 km.